First-principles study of the Bi_MO_4 antisite defect in the $Bi_{12}MO_{20}$ (M=Si, Ge, Ti) sillenite compounds

2013 J. Phys.: Condens. Matter 25 495505

(http://iopscience.iop.org/0953-8984/25/49/495505)

IOP Publishing Journal of Physics: Condensed Matter
J. Phys.: Condens. Matter **25** (2013) 495505 (9pp) doi:10.1088/0953-8984/25/49/495505

First-principles study of the Bi_MO_4 antisite defect in the $Bi_{12}MO_{20}$ (M = Si, Ge, Ti) sillenite compounds

A F Lima and M V Lalic

Departamento de Física, Universidade Federal de Sergipe, PO Box 353, 49100-000, São Cristóvão, SE, Brazil

E-mail: mlalic@ufs.br

Received 16 May 2013, in final form 11 October 2013
Published 8 November 2013
Online at stacks.iop.org/JPhysCM/25/495505

Abstract
Structural, electronic and optical properties of the antisite Bi_MO_4 defect in $Bi_{12}MO_{20}$ sillenites (BMO, M = Si, Ge, Ti) were investigated using density functional theory. The defect is studied in neutral, positively and negatively charged states. It is demonstrated that within the neutral defect the Bi $6s^2$ lone pair is broken and the valence state of the Bi is 4+ ($6s^1$). Within the charged defects, the Bi 6s orbital is found to be either full (Bi^{3+}: $6s^2$) or empty (Bi^{5+}: $6s^0$). All three charged states introduce energy bands within the BMO gap. By analyzing possible transitions between them we deduced a simple model of functioning of the Bi_MO_4 defect that is able to explain the photochromic and photorefractive effect in sillenites and that reproduces almost all known experimental facts.

(Some figures may appear in colour only in the online journal)

1. Introduction

The sillenite crystals with chemical formula $Bi_{12}MO_{20}$ (BMO, M = Ti, Ge, Si) attract significant scientific attention mostly because of their pronounced photorefractive (PR) effect that is used in many applications such as multi-wavelength holography [1], real-time holographic surface imaging [2, 3], optical information processing [4] and in various metrological problems [5]. Besides, the sillenites also exhibit pronounced optical activity and Faraday rotation, very useful properties for development of fiber optic current sensors [6, 7] and a variety of photocatalytic applications [8, 9].

A simple optical recording in PR materials requires the presence of photoconductive centers, usually defects or impurities, which provide additional energy levels within the band gap. They serve as traps for electrons which, under coherent illumination, migrate from bright to dark regions of crystal space, changing electrical and optical properties of the perfect compound [10]. Characterization of these levels and comprehension of their origin are necessary tasks for efficient manipulation and technological application of PR materials.

The nominally pure sillenites possess a complex structure of intrinsic defects [11–15], a fact proven by observation of the PR effect in undoped materials [16–18]. Summarizing [11–15], the majority of them involve wrong population of the M site (with nominal valence 4+) which can be partially (I) occupied by the Bi^{3+} ion tetrahedrally coordinated by the O ions (Bi_MO_4), (II) occupied by the Bi^{3+} ion coordinated with three O ions (Bi_MO_3) and with the Bi $6s^2$ lone pair pointing in the direction of the fourth absent O, or (III) vacant (VO_4). The Bi_MO_4 and Bi_MO_3 defect centers are commonly known as antisite Bi defects (Bi_M) in sillenites.

Even though is possible that all three types of defect coexist simultaneously, the PR effect is always justified on the basis of the Bi_MO_4 defect center [16–18]. The latter has been studied experimentally in two different states of the host crystal: (1) a bleached state (reached by thermal exposure or red light illumination of the sample), and (2) a colored state (realized by blue light illumination of the bleached sample). The following facts were established. Within the bleached state the BMOs do not exhibit any absorption from the near-infrared to ultraviolet range (the band gap in all three

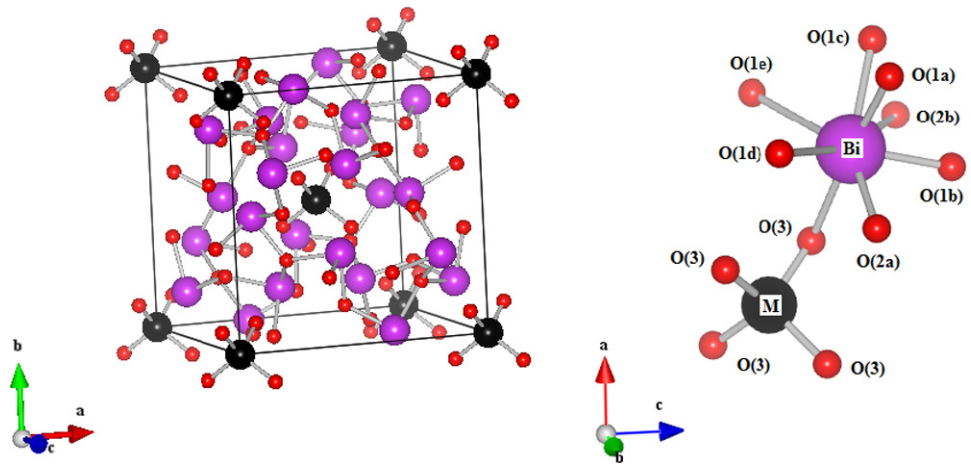

Figure 1. Crystal structure of the perfect $Bi_{12}MO_{20}$ (left) and local structure around the Bi and the M sites (right). Each Bi^{3+} ion is surrounded by eight O ions, forming a BiO_8 irregular polyhedron, whereas each M^{4+} ion is coordinated by four O(3) ions arranged in a perfect MO_4 tetrahedron.

BMOs is about 3.2 eV) [18], but a narrow shoulder is detected at approximately 3 eV near the absorption edge [10]. The fact that magnetic circular dichroism (MCD) measurements do not register this shoulder means that it is provoked by diamagnetic defect [10]. Within the colored state of the BMOs [19] the optical absorption measurements register a very intense and broad shoulder in the visible and near-infrared region [10, 20]. The MCD and optically detected magnetic resonance (ODMR) studies correlate this shoulder with the paramagnetic defect [10, 13].

In order to explain these experimental facts various theoretical models have been proposed, some of them being very complex and invoking the presence of other kind of defect in sillenites. Considering solely the structure of the Bi_MO_4 defect, however, only two of them are essentially different. Both rely on stability of the Bi $6s^2$ lone pair and suppose that in the electrically neutral state the Bi_MO_4 defect consists of the Bi in its 3+ valence state, with diamagnetic electron configuration $6s^2$, and of a hole situated in oxygen neighborhood. The first model, proposed by Oberschmid [20] and substantiated by Schirmer *et al* [21] and Briat *et al* [10], supposes that a hole is localized on one of the four neighboring O^{2-} ions, forming a bound polaron. In this case, a deformation of the perfect O tetrahedron around the Bi by elongation of one of the Bi–O bonds is expected, a fact which is not experimentally observed [13]. The second theoretical model, proposed by Reyher *et al* [11], supposes that a hole is spread equally on all four neighboring O atoms, preserving a perfect tetrahedral symmetry of the Bi_MO_4 defect. The recent EPR study [13] favors exactly this model, discarding the possibility of small polaron formation. Both models agree that in the BMO's bleached state the Bi_MO_4 defect should be neutral with the Bi ion in diamagnetic configuration $6s^2$. Blue light illumination excites one of the Bi 6s electrons into the conduction band, transforming the host into the colored state in which the Bi ion appears in paramagnetic configuration $6s^1$ and the excited electron is captured by other defects.

In this paper we suggest a substantially different model for the Bi_MO_4 defect, based on density functional theory (DFT) calculations. In the proposed model the Bi ion within the neutral defect should be in the paramagnetic $6s^1$ configuration, with a valence state of approximately 4+ (Bi_M^0). This defect is present in the colored state of the host, and acts simultaneously as electron donor and acceptor. Red light illumination charges or discharges the Bi $6s^1$ states, creating the Bi_M^- (with the Bi in the $6s^2$ configuration) or the Bi_M^+ defect (with the Bi in the $6s^0$ configuration). The bleached state of the BMOs should contain these two kinds of diamagnetic defect. The blue (or more energetic) light illumination excites electrons or holes from these defects, creating again the paramagnetic Bi_M^0 defect and transforming the host into the colored state. In the rest of the paper we will detail the theoretical foundation of this model and demonstrate that it is able to explain most of the established experimental facts.

2. Computational procedure

2.1. Simulation of isolated intrinsic defect and structural relaxation

The BMO's crystal structure is body-centered cubic, with space group I23 (no 197) [22]. The primitive unit cell contains 1 f.u. (33 atoms) without having a center of inversion. It contains three nonequivalent O atoms, one at the position 24f (O(1)), and two at the position 8c (O(2) and O(3)). The M^{4+} ion occupies 2a site, being bonded with four O(3) atoms. The local structure can be viewed as a regular tetrahedron with the M^{4+} at its center and O^{2-} at its vertices. The Bi^{3+} ions occupy the 24f site, being surrounded by eight O atoms that form a distorted BiO_8 polyhedron [32]. Within the unit cell the MO_4 tetrahedra are located at the body-centered and corner sites. Connection between the BiO_8 polyhedron and the MO_4 tetrahedron is established via the O(3) ion (figure 1).

The Bi_MO_4 defect center was simulated using the primitive unit cell of the perfect $Bi_{12}TiO_{20}$ (BTO) crystal, whose lattice parameter has been computationally relaxed

in our recent work ($a = 10.322$ Å) [23]. The BTO (and not the $Bi_{12}GeO_{20}$ (BGO) or $Bi_{12}SiO_{20}$ (BSO)) unit cell was chosen because the calculated gap agrees best with the experimental value [18]. Within this unit cell the central Ti^{4+} ion has been replaced by the Bi^{3+} ion generating the neutral antisite defect Bi^0_{Ti}. The defective periodic system BTO:Bi^0_{Ti} is then generated by infinite repetition of this unit cell, which actually does not contain the Ti ions and simulates all three BMO:Bi^0_M compounds. We estimated that this unit cell is large enough to prevent significant interaction between defects and to correctly simulate their neighborhoods (see the discussion at the end of section 4). The antisite defect is also studied in two ionization states: positively charged Bi^+_M is simulated by removing one electron from the unit cell of the BMO:Bi^0_M and negatively charged Bi^-_M by adding one electron to it. In both cases a charge compensating homogeneous *jellium* background charge is assumed to preserve overall neutrality.

For all three differently charged defective systems all atomic positions inside respective unit cells were relaxed by moving the atoms according to forces which act on them (damped Newton scheme) [24]. The process was repeated until these forces became less than 2.0 mRyd/a.u. During relaxation the symmetry constraints of the space group have been obeyed because of strong experimental evidence that the M site experiences a perfect tetrahedral crystal field [13].

2.2. Calculations of electronic structure and optical response

All calculations were carried out using a full potential linear augmented plane wave (FP-LAPW) method [25] based on DFT [26] and implemented in the WIEN2k computer code [27]. The electronic wavefunctions, charge density and crystal potential were expanded in terms of partial waves inside the non-overlapping atomic spheres centered at each nuclear position (with radii R_{MT}) and in terms of the plane waves in the rest of the space (interstitial). The choices for the Bi and O R_{MT}s were 2.3 and 1.4 a.u. respectively. The partial waves were expanded up to $l_{max} = 10$, while the number of plane waves was limited by the cut-off at $K_{max} = 7.0/R_{MT}(O)$. As a basis, the augmented plane waves were used. The charge density was Fourier expanded up to $G_{max} = 14$. A mesh of seven k-points in the irreducible part of the Brillouin zone was used. The Bi 5d, 6s, 6p and the O 2s, 2p electronic states were considered as valence ones and treated within the scalar-relativistic approach, whereas the core states were relaxed in a fully relativistic manner.

Exchange and correlation effects were treated in a twofold manner. The relaxation of atomic positions has been performed using the generalized gradient approximation with Perdew–Burke–Ernzerhof parameterization (GGA-PBE) [28]. While this functional is very useful in calculating structural and other properties related to total energies, it severely underestimates the band gaps of most semiconductors and insulators. Thus, electronic bands and optical response have been calculated using the semi-local modified Becke–Johnson (mBJ) functional recently proposed by Tran and Blaha [29]. This functional has been shown to reproduce better the band gaps, electronic and optical properties for a variety of semiconductors and insulators [30–32]. The spin–orbit coupling has been taken into account just for heavy Bi atoms via a second variation procedure, using scalar-relativistic eigenfunctions as a basis. Electronic structure was calculated up to an energy of 4.0 Ryd. The self-consistent calculations of all three defective systems were performed on the same level of precision and successfully converged within the energy precision of 10^{-5} Ryd.

The linear optical properties were determined by the WIEN2k optical package [33], which calculates the imaginary part of the complex dielectric tensor ε_2, directly proportional to the optical absorption spectrum, on the basis of the following formula [34]:

$$\varepsilon_{2(\alpha\beta)}(\omega) = \frac{4\pi^2 e^2}{m^2\omega^2}\sum_{i,f}\int_{BZ}\frac{2dk}{(2\pi)^3}|\langle\varphi_{fk}|P_\beta|\varphi_{ik}\rangle| \times |\langle\varphi_{fk}|P_\alpha|\varphi_{ik}\rangle|\delta[E_f(k) - E_i(k) - \hbar\omega]. \quad (1)$$

Formula (1) is valid within the frame of the random phase approximation and does not account for electron polarization effects. It therefore cannot describe excitonic effects, but in the case of sillenites there are no experimental proofs of their importance. Instead, it describes electric dipole allowed transitions from populated Kohn–Sham states $|\varphi_{ik}\rangle$ of energy $E_i(k)$ to empty Kohn–Sham states $|\varphi_{fk}\rangle$ of energy $E_f(k)$ with the same wavevector k (ω is the frequency of incident radiation, m the electron mass, P the momentum operator, and α and β stand for the projections x, y or z). ε_2 was computed in the energy range from 0 to 3 Ryd (0–40 eV), taking into account electronic transitions from -1.2 to 2.0 Ryd. The number of empty states considered was approximately 254, for all three defective systems. A mesh of 45 k-points in the irreducible wedge of the first Brillouin zone was used. Owing to their cubic symmetry, the sillenite's dielectric tensor is diagonal, with $\varepsilon_{2xx} = \varepsilon_{2yy} = \varepsilon_{2zz} = \varepsilon_2$, and thus reduced to scalar function $\varepsilon_2(\omega)$.

3. Results and discussion

3.1. Electronic structure of defective systems

Resulting total and partial densities of electronic states (TDOS and PDOS) of the three BMO:$Bi^{0,1+,1-}_M$ defective systems are presented in figure 2, together with the TDOS of the perfect BTO (calculated recently by our group [32]), which is shown for comparison.

For the perfect BTO the calculated gap was 0.243 Ryd (3.3 eV), very close to the experimental value of 3.2 eV [18]. The peak at the very top of the valence band (marked by letter A) is predominantly composed of the 2p states of the O(3) and the Bi 6s states. The peak at the very bottom of the conduction band (marked by B) is dominated by the Bi 6p states hybridized with the 2p states of the O atoms [32].

For the defective systems, figure 2 reveals two principal differences relative to the perfect one: (1) significant change of intensity, form and composition of the TDOS at the top of the valence band, and (2) formation of one extra band, situated within the fundamental gap and composed of the hybridized Bi_M 6s and O(3) 2p states.

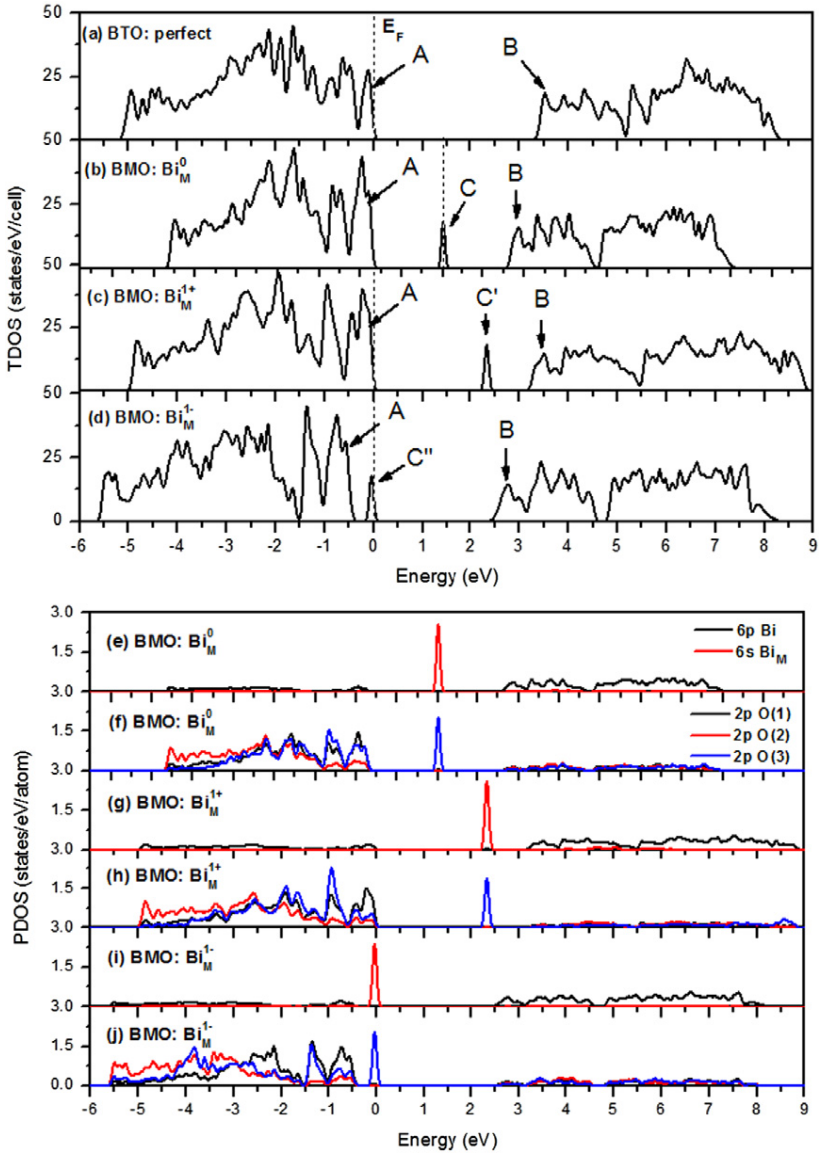

Figure 2. Top: calculated TDOS of the perfect BTO (a) and the BMO containing the neutral (b), positively (c) and negatively (d) charged antisite Bi_M defect. The letters A and B denote the peaks at the valence band top and conduction band bottom, respectively. The letters C, C′ and C″ denote bands within the gap introduced by the antisite defect. The dashed line indicates the Fermi energy. Bottom: calculated PDOS of the three defective BMO crystals. A band due to the antisite Bi defect is composed of a mixture of the Bi_M 6s and the O(3) 2p states.

The first difference can be related to the relaxation of atomic positions in defective systems. In perfect BMOs the shortest bonds are the M–O(3) ones, so the occupied O(3) states have high energy and dominate the very top of the valence band [32]. In defective systems the Bi_M–O(3) bonds are significantly elongated (see table 1), and the Bi–O(1) bonds become the shortest ones (since the neighborhood around the regular Bi sites in defective systems does not change much we did not find it necessary to represent a table with the Bi–O interatomic distances; this table for the pure BMOs can be consulted in [32]). As a consequence, the dominant orbital character of the valence band top in defective systems changes from the O(3) to the O(1) 2p states, while the TDOS intensity increases because there are more O(1) than O(3) atoms within the BMO unit cell.

Table 1. Calculated equilibrium distances between the Bi_M^q defects and their nearest and next-nearest (NN and NNN) neighboring O atoms, as well as between the Bi_M^q and the nearest regular Bi ions. The same distances in the pure BTO are shown in the last line, taken from [23].

	Distances (Å)		
	NN O atoms O(3)	NNN O atoms O(2b)	Bi_M^q–Bi
Bi_M^0	2.112	3.901	3.925
Bi_M^+	2.026	3.988	3.980
Bi_M^-	2.200	3.645	3.836
Ti	1.842	3.443	3.913

The second difference is a fundamental one, resulting in formation of a new permitted energy band within the gap. In all three defective systems this band can admit up to two

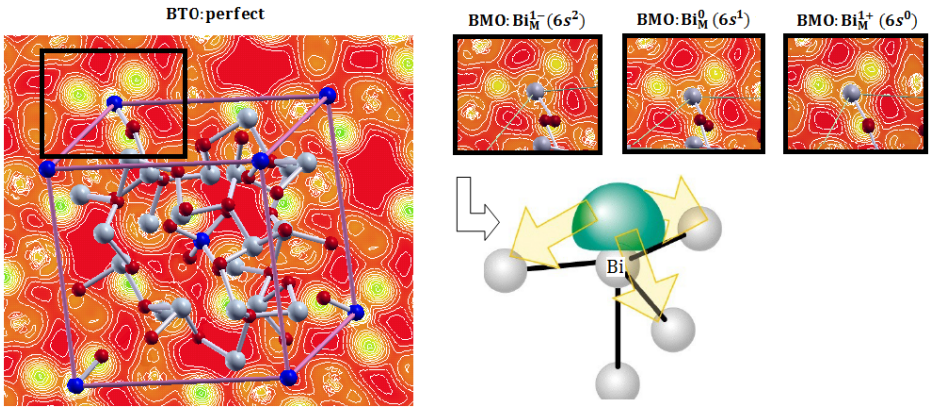

Figure 3. Valence electron density of the Bi_MO_4 defect projected onto the (111) crystal plane. In the left picture the black frame emphasizes the TiO_4 cluster within the perfect BTO: the Ti ion is in the center, and its three neighboring O atoms have density projections around it (they are actually slightly above the plane). The fourth O is exactly below the Ti and therefore not seen. The three pictures on the right refer to the differently charged Bi_M defects and demonstrate deterioration of the Bi_M $6s^2$ lone pair. The sketch below these pictures illustrates the form of the $6s^2$ electronic cloud, facilitating the visualization of its projection onto the plane formed by the Bi and three neighboring O atoms.

electrons, but its actual occupation and energy depend on the charge state of the defect.

The neutral defect (figure 2(b)) forms a deep, half-occupied band, placed in the middle of the gap. Since this band has the dominant Bi 6s character (figure 2(e)), it can be concluded that the Bi releases one electron from its $6s^2$ lone pair to satisfy bonding with all four neighboring O(3) ions. Thus, four of the five valence electrons of the Bi ($6s^26p^3$ in free-atom configuration) are used to form the tetrahedral covalent bonds with the neighbors, while the fifth electron remains within the Bi_M atomic sphere. This fact can be interpreted as if the Bi ion within the Bi_M^0 defect exhibits approximately the $6s^1$ configuration, being in the valence state 4+. It introduces both donor and acceptor states into the BMO's gap.

The positively charged Bi_M^+ defect forms an acceptor band (figure 2(c)). Since it has predominantly the Bi 6s character (figure 2(g)), this result indicates that one electron has been removed from the Bi 6s orbital, leaving the Bi without any valence electrons. This situation describes the 5+ valence state of the Bi ($6s^0$ configuration). It is physically realized when the Bi $6s^1$ electron is excited to the conduction band by, for example, an optical absorption process.

The negatively charged Bi_M^- defect introduces a donor band within the BMO gap (figure 2(d)). Again, the fact that the band exhibits predominant Bi 6s character (figure 2(i)) leads to the conclusion that one extra electron is accommodated into the Bi $6s^2$ orbital, recuperating the Bi $6s^2$ lone pair. Thus, the formal valence of the Bi ion within the Bi_M^- defect is 3+ ($6s^2$ configuration). This defect is realized when the neutral Bi_M^0 defect captures an electron from somewhere, either by excitation from the valence band top or by de-excitation from the conduction band bottom. In the first case the 2p electron is transferred to the Bi from the O(3) surrounding it, while in the second case the additional electron is captured from other regions of the crystal (possibly originating from other defects).

Contrary to existing models, our theoretical results predict vulnerability of the Bi $6s^2$ lone pair within the Bi_MO_4 defect. Our calculations clearly indicate that within the Bi_M^0 defect the Bi uses one of its 6s electrons to satisfy the missing (fourth) bond with neighboring O atoms without producing an electron hole but, instead, changing its valence state from 3+ to 4+. The results of simulation of the charged defects additionally support 'vulnerability' of the Bi $6s^2$ states (in the sense of their facility to be occupied or unoccupied). Namely, the charged defects were simulated by addition or subtraction of one electron in the reference of the whole unit cell of the BMO. During the calculations this electron (or hole) was redistributed in the manner that leads to convergent solution of the Kohn–Sham equations. As a result, the extra (or missing) electron is always localized within the Bi_M–O(3) bonds, i.e. by filling (or emptying) the 6s orbital of the Bi ion. This fact is illustrated in figure 3.

3.2. Energetic and structural characteristics of the Bi_MO_4 defect

In order to check if all three Bi_M^q defects are physically realizable and to estimate their relative stabilities, we need to calculate their formation energies. In the present study the reference pure system is the BTO (see discussion in the section 2.1), and thus we are able to discuss only defect formation energies in this compound: Bi_{Ti}^q. The results, however, could be somewhat generalized for the antisite defects in the other two sillenites (BGO and BSO), considering the fact that the Ge and Si ions have the same valence state (4+) and the same surroundings as the Ti ions in the BTO. Formation energies of the Bi_{Ti}^q defects are calculated on the basis of the following formula [35, 36]:

$$E_f(\mathrm{BTO{:}Bi}_{\mathrm{Ti}}^q) = E_{\mathrm{T}}(\mathrm{BTO{:}Bi}_{\mathrm{Ti}}^q) - E_{\mathrm{T}}(\mathrm{BTO}) + \mu_{\mathrm{Ti}} - \mu_{\mathrm{Bi}} + q(E_{\mathrm{VBM}} + E_{\mathrm{F}} + \Delta V^{(q)}) \quad (2)$$

where the first two terms on the right-hand side represent the total energies of the perfect and defect-containing BTO

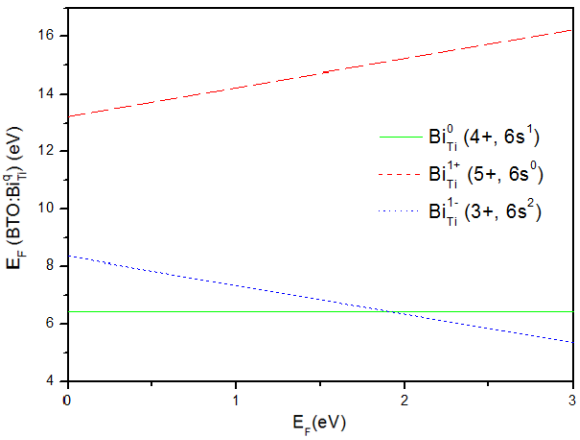

Figure 4. Formation energies of the Bi^{q}_{Ti} defects as functions of Fermi energy (calculated from the top of the valence band).

cells, the third and fourth terms are chemical potentials of the atoms which are removed (Ti) and added (Bi) to form the defective system, and the fifth term is the electron chemical potential. In the last term q is the charge state of the defect $(-1, 0, +1)$, E_{VBM} is the energy of the valence band maximum (VBM) of the perfect BTO system, E_F is the Fermi energy counted with respect to the E_{VBM}, and ΔV is the difference between average electrostatic potentials in the perfect and defective unit cells (needed to provide the same reference level for E_{VBM} in different systems). The μ_{Ti} and μ_{Bi} are estimated from their upper bounds, i.e. they are calculated as energies per atom for bulk hexagonal close packed metallic Ti and orthorhombic metallic Bi. All terms in equation (2) are computed using the TB-mBJ exchange–correlation potential.

The formation energy of the Bi^{0}_{Ti} defect was calculated to be +6.42 eV, while the formation energies of the Bi^{+}_{Ti} and Bi^{-}_{Ti} defects were determined as 13.23 eV + E_F and 8.35 eV − E_F respectively. From these results it is possible to analyze the relative stabilities of the charged defects compared to the neutral one, as shown in figure 4.

From figure 4 one can conclude that the neutral defect is the most stable one over the range of Fermi energies from 0 to 2 eV, while the negative defect becomes energetically favorable for Fermi energies between 2 and 3.3 eV. The positively charged defect is the most difficult to realize over the whole range of possible Fermi energies.

Table 1 summarizes the calculated inter-ionic distances between differently charged antisite Bi defects and their nearest and next-nearest (NN and NNN) neighboring O atoms, as well as the distances between Bi^{q}_{M} and their nearest Bi ions. For comparison the same distances are listed for the Ti ion in the perfect BTO. The Ti has the four O(3) ions as the first and the four O(2b) atoms as the second NNs. This ordering is preserved for the Bi^{0}_{M} and Bi^{-}_{M} defects, but not for the Bi^{+}_{M} defect, for which the second neighborhood consists of the 12 Bi atoms at the distance of 3.980 Å, while four O(2b) appear at the distance of 3.988 Å as the third neighbors.

Table 1 exhibits some useful pieces of information about the structural properties of three defective BMO systems. First, it shows that all defects induce considerable expansion of their first and second coordination spheres as compared with the perfect system. Second, it expresses a clear dependence of interatomic distances on the charge state of the defects. If the neutral defect Bi^{0}_{M} is considered as a referent system for comparison, then the Bi^{+}_{M} produces smaller expansion of its first and larger expansion of its second coordination sphere. On the other hand, the Bi^{-}_{M} defect induces larger expansion of its first and smaller expansion of its second coordination sphere. The Bi^{q}_{M}–Bi distances exhibit the same trend as the Bi^{q}_{M}–O(2b) ones.

All these characteristics can be understood on the basis of electronic configurations of three Bi^{q}_{M} defects deduced from electronic structure calculations presented in section 3.1. Within the neutral Bi^{0}_{M} defect the Bi appears in the formal valence state 4+. It repulses the NN and the NNN O atoms for two reasons: (1) the ionic radius of the Bi is much larger than the M, and (2) the presence of a spatially extended $6s^1$ negative cloud additionally repels the negative oxygen ions. Within the negatively charged Bi^{-}_{M} defect, the Bi is in the formal valence state 3+. A spatially extended $6s^2$ electron cloud is more negative, thus the Bi^{3+} repels the NN O atoms farther away than the Bi^{4+}. At the same time, the Bi^{3+} repels the NNN O(2b) atoms less than the Bi^{4+} due to a weaker electrostatic interaction with the neighboring Bi^{3+} ions at the regular crystallographic sites (the Bi^{3+}–Bi^{3+} electrostatic repulsion is weaker than the Bi^{4+}–Bi^{3+} one). The O(2b) atoms, being the NNs of the regular Bi^{3+}, are simply dragged together with the regular Bi^{3+} since they are bound much more strongly to it. Within the positively charged Bi^{+}_{M} defect the valence state of the Bi is 5+. Owing to the lack of the 6s negative electron cloud the Bi^{5+}–O(3) bonds are shorter in comparison with the neutral defect. At the same time, the Bi^{5+}–Bi^{3+} electrostatic repulsion is stronger than the Bi^{3+}–Bi^{3+} repulsion, and the Bi^{5+}–O(2b) bonds are considerably longer than in the case of the neutral defect.

3.3. Optical absorption spectra of defective systems

The presence of antisite defects causes changes in the absorption spectrum of the BMOs, and these changes are most pronounced near the optical absorption edge of the perfect system. Figure 5 shows the calculated imaginary part of the dielectric function ε_2 of the three BMO:Bi^{q}_{M} defective systems, as well as of the perfect BTO, as a function of incident radiation energy in the range of 1.5–4.0 eV.

As can be seen from figure 5, the perfect material starts to absorb the photons at the energy of 3.3 eV, while the spectra of all defective systems are characterized by prominent peaks below this energy. These peaks can be interpreted in terms of electronic structures presented in figure 2. The peaks I, I′ and I″ in the BMO:Bi^{0}_{M} spectrum are formed by electronic transitions from band A to band C and from band C to band B. Taking into account the distance between atoms and predominant orbital character of the bands A, B and C, these structures are mainly determined by transitions from the O(3) 2p to the Bi_M 6s, from the O(3) 2p to the Bi_M 6p-, and from the Bi 6s to the O(3) 2p and the Bi_M 6p states. All these

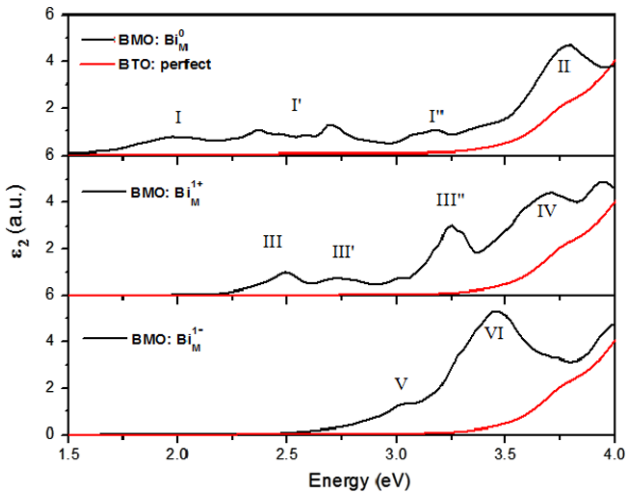

Figure 5. Imaginary part of dielectric function of the perfect BTO (red line) and the BMO containing an antisite Bi defect in three different charge states (black lines) as a function of incident radiation energy. The prominent structures on the spectra are denoted by roman numbers I–VI.

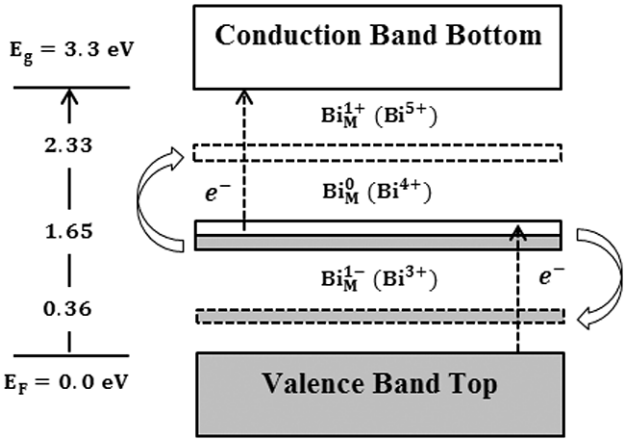

Figure 6. Schematic representation of energy bands formed by antisite defects Bi_M^q in the BMOs. The arrows indicate possible processes that ionize the Bi_M^0 defect center leading to the formation of a donor (Bi_M^-) or acceptor (Bi_M^+) band.

transitions transform the Bi electronic configuration from $6s^1$ to $6s^2$ (Bi^{3+} ion) and $6s^0$ (Bi^{5+} ion), creating the Bi_M^- and the Bi_M^+ antisite defects. The optical spectrum of BMO:Bi_M^+ also exhibits three prominent peaks (III, III′ and III″) below the absorption threshold of the perfect BTO. These structures are due to electronic transitions from the top of the valence band A to the unoccupied band C′ within the gap. The electronic transitions involved are those between the O(3) 2p and the Bi 6s states. The optical spectrum of the BMO:Bi_M^- defect exhibits only one peak, numbered as V, below the absorption edge of the pure BTO. It is formed by electron transfer from band C″ (occupied Bi 6s and O(3) 2p states) to band B (unoccupied O(3) 2p and the Bi 6p states).

Figure 5 also demonstrates that optical absorption above the 3.3 eV is more intense in defective systems than in the perfect BMOs. This characteristic is emphasized by peaks II (figure 5(a)), IV (figure 5(b)) and VI (figure 5(c)). It can be related to the existence of the higher DOS at the top of the valence band of defective systems (figures 2(b)–(d)) compared to the perfect BTO (figure 2(a)). This occurs because the O(1) 2p states become dominant at the valence band top of the defective systems (as discussed in section 3.1), increasing the probability of optical transition between the Bi and O(1) within the regular BiO_8 polyhedron.

4. Model of the Bi_MO_4 defect

On the basis of results presented in section 3.3, it is possible to construct a model of the functioning of the antisite Bi_MO_4 defect that is able to explain the photochromic and PR effect in sillenites and that agrees with most of the basic experimental facts established so far. Deduction of the model can be assisted by a schematic representation of energy bands within the BMO gap originated from the Bi_M^q defects, as shown in figure 6. The scheme is constructed on the basis of the electronic structure presented in figures 2(b)–(d).

The neutral Bi_M^0 is the defect that exists in the BMOs which are not subjected to any treatment, i.e. in their so-called colored state. This defect is paramagnetic (Bi^{4+}: $6s^1$), a fact that agrees with MCD and ODMR experiments realized in the colored state [10, 13]. It creates a semi-populated deep energy band in the middle of the gap, whose center is at approximately 1.65 eV counted from the valence band top. Under appropriate illumination (or other kind of excitation) that provides at least this amount of energy, one electron can be released from this center to the conduction band, giving rise to the positively charged Bi_M^+ defect, or one electron can be captured by it, forming the negatively charged Bi_M^- defect (figure 6). In the first case an acceptor band is created, 0.97 eV below the conduction band bottom. In the second case, a donor band is formed 0.36 eV above the valence band top. The longer an energy excitation lasts, the higher is the probability of creating the donor and acceptor bands. After some time of continuous excitation, the deep band should be completely erased and the crystal transformed into another state, in which just the Bi_M^- and Bi_M^+ defects exist. Both are diamagnetic defects, with the Bi ion configuration $6s^2$ and $6s^0$ respectively. The new state of crystal is optically (or thermally) treated, bleached state. The predicted transformation from colored to bleached state agrees with the experimental findings that red light (1.65–2.0 eV) illumination or short thermal annealing (10–20 min at ∼500 C) transforms the BMO from colored to bleached state, in which diamagnetic defects prevail [10, 19]. The reverse transformation, from bleached to colored state, can be performed either by excitation of an electron from the valence band top to the acceptor band (∼2.33 eV) or by excitation from the donor band to the conduction band bottom (∼2.97 eV). In both cases, the Bi_M^+ and the Bi_M^- defects are discharged, the donor and acceptor bands erased and the paramagnetic deep band restored in the center of the gap. This process is also in agreement with experimental findings that blue (2.50–2.85 eV) [19] or violet (2.85–3.25 eV) [10] light illumination transforms the BMO from bleached to colored state.

The presented model emphasizes the importance of the Bi_MO_4 defect for explanation of the PR effect in sillenites. Under coherent illumination of the crystal this defect acts as a donor and acceptor of the electrons at the same time (Bi_M^0), providing the traps for electrons (Bi_M^+) and holes (Bi_M^-) throughout the lattice, fulfilling in this way essential conditions required for optical recording via space–charge modulation [16–18].

Considering the optical absorption process caused by antisite defects, the presented model predicts the following features.

In the bleached state, optical absorption of the BMO's below gap energy should be composed of superposition of the Bi_M^+ and the Bi_M^- ε_2 spectra shown in figure 5. This superposition results in peaks centered at approximately 2.50, 2.75 and 3.00 eV. The experiment, however, observes just the shoulder at the energy of ∼3 eV [10]. There are two possible reasons for this disagreement: (1) optical calculations overestimated the transition probability from the O(3) 2p to the Bi_M 6s states (those which generate peaks at 2.5 and 2.75 eV), resulting in higher absorption intensity than measured; (2) owing to the relatively small supercell size and approximate treatment of exchange–correlation effects in our calculations the energy of the acceptor band is slightly underestimated; if this band were positioned ∼0.5 eV higher in energy, the peak at 2.5 eV would be centered on 3 eV while other peaks would be immersed into the host absorption.

In the colored state, the BMO's optical absorption edge should be influenced only by neutral defects and absorption described by the ε_2 spectrum of the Bi_M^0 (figure 5). In the literature, however, the optical absorption spectrum of the BMOs at room temperature is sometimes presented [20], in which case it should be composed of a superposition of all three spectra shown in figure 5 (since all three differently charged defects should coexist in the host). In both cases our theoretical model predicts formation of a broad shoulder in the optical absorption spectrum of the BMO, as shown in figure 7, which explains the coloration of the material provoked by proper illumination (photochromism). It also demonstrates good qualitative agreement with experimental results.

It is worth mentioning that several experimental studies of doped sillenites have discussed the change of valence state of the impurities after illumination and its influence on the photoconductivity and photochromicity of the material. Montenegro *et al* [37] and Carvalho *et al* [38] studied optical absorption of nominally pure BTO doped with V atoms. They suggested that some of the tetrahedral sites occupied by Bi^{4+} defects may be substituted by either V^{3+} or V^{5+} ions. A similar conclusion is also drawn from works of Marquet *et al* [19] and McCullough *et al* [39], who investigated the optical absorption of BGO doped with Cr. Our theoretical study clearly substantiates their suggestions.

Finally, let us briefly discuss the reliability of the calculations presented in this paper. It is a fact that the size of the supercell used to simulate antisite defects was not very large (this is especially valid for consideration of the charged defects). This size is, however, sufficient to constrain the geometric influence of the defects within the supercell, as can be seen from the following facts.

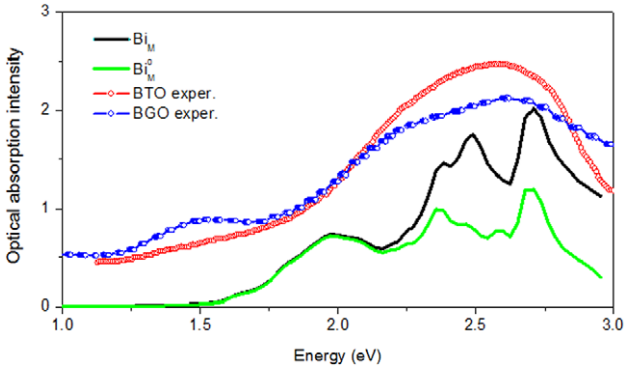

Figure 7. Calculated optical absorption spectra of the BMO in the colored state (green line) and in the state in which all three Bi_M^q defects coexist (black line). They are compared to measured absorption spectra of nominally undoped BTO (red curve, [21]) and BGO (blue curve, [10]). The theoretical spectra are calculated in the energy range 0–3 eV, simulating measurements which were made up to this energy.

(1) Analysis of interatomic distances has shown that the lattice deformation is localized nearby the defect. Table 1 demonstrates that the distances between the defect and its neighboring O atoms are changed very much, which is not the case with distances between the defect and its third-neighboring Bi. The distances between the defect and the atoms situated farther away (not shown in the paper due to economy of space) are quite similar to the distances in the pure compound, for all three kinds of defect considered.

(2) Electronic bands of the defects, introduced within the band gap, are narrow. The thicknesses of the neutral and the charged defects' bands are similar (figure 2). This fact indicates very small overlap between the wavefunction of the defect and its periodic images in other supercells.

(3) According to the distribution of the valence charge density, shown in figure 3, an extra or a missing electron charge (within the charged defects) is concentrated nearby the defect, populating or emptying the 6s states of the Bi.

The supercell size used in the present study is also sufficient to significantly reduce the magnitude of the Coulomb interaction between the charged defect and its periodic images. This effect can be estimated by calculating the first term of the Makov–Payne correction to the energy of the ionic crystals [40] (written in SI units):

$$E_{\mathrm{corr}}^{\mathrm{MP}} = \frac{1}{4\pi\varepsilon_0\varepsilon_{\mathrm{r}}}\frac{q^2\alpha}{2L} \tag{3}$$

where $q = \pm e$ (charges), $\alpha = 3.64$ (Madelung constant for bcc lattice), $L = 10.322$ Å (supercell lattice constant) and $\varepsilon_{\mathrm{r}} \approx 50$ (static dielectric constants of the BTO, BSO and BGO are 48, 56 and 47 respectively [41]). The result obtained is $E_{\mathrm{corr}} = 50$ meV. Thus, even though the supercell is not large, due to the high dielectric constant of the sillenites the Coulomb interaction between defects is strongly screened and, consequently, errors in calculated total energies and positions of the Kohn–Sham bands within the gap are small.

5. Conclusions

In this paper we performed a thorough theoretical study of the antisite Bi_MO_4 defect in the $Bi_{12}MO_{20}$ (M = Si, Ge, Ti; BMO) sillenite compounds, which is formed by wrong occupation of the M^{4+} sites by the Bi^{3+} ions (Bi_M). As a tool we used the first-principles FP-(L)APW method, based on DFT and implemented in the WIEN2k computer code. We discussed the structural, electronic and optical properties of the Bi_M defect in its neutral (Bi_M^0), negative (Bi_M^-) and positive (Bi_M^+) charge state.

The results of our study demonstrate that within the neutral defect (Bi_M^0) the Bi $6s^2$ lone pair is broken and the Bi electron configuration is $6s^1$. By capturing or emitting one electron, the Bi assumes $6s^2$ or $6s^0$ configurations respectively, forming the Bi_M^- and Bi_M^+ charged defects. All three Bi_M^q defects introduce bands inside the BMO gap: the Bi_M^0 a half-occupied deep band, the Bi_M^- a donor band and the Bi_M^+ an acceptor band. By analyzing the interplay of possible transitions between them we deduced a model of functioning of the Bi_M defect in sillenites which is substantially different from the existing ones. In brief, our model predicts that the Bi_M^0 defect should be dominant in the colored state of the BMOs and should act simultaneously as a donor and an acceptor. Under proper excitation it can create traps for electrons (Bi_M^+) and holes (Bi_M^-) throughout the lattice, transforming the host into the bleached state and fulfilling the basic conditions required for optical recording via space–charge modulation. The model explains the domination of paramagnetic defects in the colored and diamagnetic defects in the bleached state, and accurately reproduces conditions that are necessary to transform the colored state into the bleached one and vice versa. Additionally, it correctly predicts the formation of the broad and intense shoulder below the optical absorption edge of the BMOs, explaining their coloration under appropriate illumination.

Acknowledgments

The authors acknowledge the CNPq, CAPES and FAPITEC (Brazilian funding agencies) for financial help. We also thank Professor J Frejlich for fruitful discussions.

References

[1] Barbosa E A, Verzini R and Carvalho J F 2006 *Opt. Commun.* **263** 189
[2] Gesualdi M R R, Soga D and Muramatsu M 2007 *Opt. Laser Technol.* **39** 98
[3] Marinova V, Liu R C, Lin S H and Hsu K Y 2011 *Opt. Lett.* **36** 1981
[4] Georges M P, Scauflaire V S and Lemaire P C 2001 *Appl. Phys.* B **72** 761
[5] Baade T, Kiessling A and Kowarschik R 2001 *J. Opt. A: Pure Appl. Opt.* **3** 250
[6] Mihailovic P, Petricevic S, Stankovic S and Radunovic J 2008 *Opt. Mater.* **30** 1079
[7] Efremidis A T, Deliolanis N C, Manolikas C and Vanidhis E D 2009 *Appl. Phys.* B **95** 467
[8] Yao W F, Wang H, Xu X H, Zhou J T, Yang X N, Zhang Y, Shang S X and Wang M 2003 *Chem. Phys. Lett.* **377** 501
[9] He C and Gu G 2006 *Scr. Mater.* **54** 1221
[10] Briat B, Grachev V G, Malovichko G I, Schirmer O F and Wöhlecke M 2006 *Photorefractive Materials and their Applications* vol 2, ed P Günter and J P Huignard (Berlin: Springer)
[11] Reyher H-J, Hellwig U and Thiemann O 1993 *Phys. Rev.* B **47** 5638
[12] Briat B, Reyher H-J, Hamri A, Romanov N G, Launay J C and Ramaz F J 1995 *J. Phys.: Condens. Matter* **7** 6951
[13] Ahmad I, Marinova V and Goovaerts E 2009 *Phys. Rev.* B **79** 033107
[14] Valant M and Suvorov D 2002 *Chem. Mater.* **14** 3471
[15] Egorysheva A V 2009 *Inorg. Mater.* **45** 1253
[16] Vogt H, Buse K, Hesse H and Kratzig E 2001 *J. Appl. Phys.* **90** 3167
[17] Frejlich J, Montenegro R, Inocente N R Jr and Santos P V 2007 *J. Appl. Phys.* **101** 043101
[18] Frejlich J, Montenegro R, Santos T O and Carvalho J F 2008 *J. Opt. A: Pure Appl. Opt.* **10** 104005
[19] Marquet H, Tapiero M, Merle J C, Zielinger J P and Launay J C 1998 *Opt. Mater.* **11** 53
[20] Oberschmid R 1985 *Phys Status Solidi* a **89** 263
[21] Schirmer O F 2006 *J. Phys.: Condens. Matter* **18** R667
[22] Efediev Sh M, Bagiev V E, Zeinally A C, Balashov V, Lomonov V and Majer A 1982 *Phys. Status Solidi* a **74** 17
[23] Lima A F and Lalic M V 2010 *Comput. Mater. Sci.* **49** 321
[24] Kohler B, Wilke S, Scheffler M, Kouba R and Ambroseh-Drax C 1996 *Comput. Phys. Commun.* **94** 31
[25] Andersen O K 1975 *Phys. Rev.* B **12** 3060
[26] Hohenberg P and Kohn W 1964 *Phys. Rev.* **136** B864
Kohn W and Sham L J 1965 *Phys. Rev.* **140** A1133
[27] Blaha P, Schwarz K, Madsen G K H, Kvasnicka D and Luitz J 2001 *An Augmented Plane Waves + Local Orbital Program for Calculating Crystal Properties* (Austria: Karlheinz Schwarz, Technische Universitat Wien)
[28] Perdew J P, Burke K and Ernzerhof M 1996 *Phys. Rev. Lett.* **77** 3865
[29] Tran F and Blaha P 2009 *Phys. Rev. Lett.* **102** 226401
[30] Singh D J, Seo S S A and Lee H N 2010 *Phys. Rev.* B **82** 180103
[31] Koller D, Tran F and Blaha P 2011 *Phys. Rev.* B **83** 195134
[32] Lima A F, Farias S A S and Lalic M V 2011 *J. Appl. Phys.* **110** 083705
[33] Ambrosch-Draxl C and Sofo J O 2006 *Comput. Phys. Commun.* **175** 1
[34] Bass M, Stryland E W V, Willians D R and Woffe W L 1995 *Handbook of Optics* 2nd edn, vol 1 (New York: McGraw-Hill)
[35] Van de Walle C G and Neugebauer J 2004 *J. Appl. Phys.* **95** 3851
[36] Komsa H-P, Rantala T T and Pasquarello A 2012 *Phys. Rev.* B **86** 045112
[37] Montenegro R, Shumelyuk A, Kumamoto R, Carvalho J F, Santana R C and Frejlich J 2009 *J. Appl. Phys.* B **95** 475
[38] Carvalho J F, Franco R W A, Magon C J, Nunes L A O and Hernandes A C 1999 *Opt. Mater.* **13** 333
[39] McCullough J S, Bauer A L H, Hunt C A and Martin J J 2001 *J. Appl. Phys.* **90** 6017
[40] Makov G and Payne M C 1995 *Phys. Rev.* B **51** 4014
[41] Bass M 1995 *Handbook of Optics* vol 2 (New York: McGraw-Hill) chapter 39